Crystallization, Orientation and Solid - Solid Crystal Transition of Polybutene-1 Confined within Nanoporous Alumina

Guangyu Shi[1,2 #], Zefan Wang[1,2 #], Ming Wang[1,2], Guoming Liu*[1,2], Dario Cavallo[3], Alejandro J. Müller[4,5] and Dujin Wang[1,2]

1. Beijing National Laboratory for Molecular Sciences, CAS Key Laboratory of Engineering Plastics, CAS Research/Education Center for Excellence in Molecular Sciences, Institute of Chemistry, Chinese Academy of Sciences, Beijing 100190, China
2. University of Chinese Academy of Sciences, Beijing 100049, China
3. Department of Chemistry and Industrial Chemistry, University of Genova, via Dodecaneso, 31, 16146 Genova, Italy
4. POLYMAT and Polymer Science and Technology Department, Faculty of Chemistry, University of the Basque Country UPV/EHU, Paseo Manuel de Lardizabal 3, 20018 Donostia-San Sebastián, Spain
5. IKERBASQUE, Basque Foundation for Science, Bilbao 48013, Spain

# equal contribution

* corresponding author: gmliu@iccas.ac.cn

ABSTRACT

The effect of confinement on the crystallization, crystal orientation, and polymorphic crystal transition of bulk and infiltrated polybutene-1 (PB-1) within nanoporous alumina templates (AAO) were studied. After cooling from the melt, PB-1 within AAO templates crystallized into the tetragonal Form II directly. The nucleation process inside the AAO pores was probably homogeneous when pore sizes were below 200 nm. The crystal orientation of Form II was investigated by grazing angle X-ray scattering. Form II to I transition was investigated as a function of time and modeled with the Avrami equation. The rate of Form II to I transition for infiltrated PB-1 within 400 nm AAO was unexpectedly higher than that of the bulk. The stress generated due to the mismatch of the thermal expansion coefficients between PB-1 and AAO greatly enhanced the nucleation of Form I within the Form II matrix. A slower Form II to I transition was observed when the pore diameter of AAO decreased. The transition degree decreased with decreasing pore diameter and was completely inhibited for PB-1 infiltrated within the 30 nm AAO template. A stable Form II interfacial layer with a thickness of ~ 12 nm was postulated to account for this phenomenon.

1. INTRODUCTION

Isotactic polybutene-1 (PB-1) is a semi-crystalline polyolefin that exhibits excellent mechanical performance, such as high modulus, stiffness, and creep resistance.[1] Four different crystalline structures have been reported for PB-1; namely, I, II, III, and I'.[2, 3] Form II, characterized by a 11_3 helical conformation in a tetragonal unit cell, can be obtained by crystallization from the melt and shows a melting temperature of 100-120 ℃.[1, 4] Form II spontaneously transforms into the more stable Form I during annealing.[5, 6] Form I has a 3_1 helical conformation in a trigonal cell and a melting temperature of 121 ~ 136 ℃.[1, 7] The Form II to I transition results in a 14 % increase in repeating length along the chain axis and a 10% cross-sectional decrease.[1] Another modification, termed as Form I', exhibits the same crystalline structure but a lower melting temperature (90 ~ 100 ℃) as compared to Form I.[8]

The Form II to I polymorphic transition is of particular interest in PB-1 as it occurs at room

temperature in the solid-state, representing a unique case for semi-crystalline polymers. Parts made with PB-1 have time-dependent dimensions and mechanical properties, as the crystal transformation is slow, and these time-dependent effects can affect practical applications. Normally, Form II to I transition completes within several days during storage at ambient temperature.[9]

For practical applications, it would be ideal if Form I/I' can be obtained directly or the transition can be greatly accelerated.[10-12] Polymorphism selection may be strongly influenced by spatial confinement.[13-15] Considering that at certain crystallization temperature the size (thickness) of Form II nuclei is much larger than that of Form I' and the growth rate of Form II is much faster than Form I', therefore, in order to obtain Form I', one needs to suppress the nucleation of Form II. This effect has been observed in butene-1/ethylene copolymers via the formation of heterogeneous melt structure after melting the original crystals.[13]

Many factors can accelerate the transition, such as quenching,[16] high pressure,[17] external or internal stress,[5, 18-21] or the introduction of 1-alkene co-monomers less than five carbon atoms.[22] A series of carefully designed DSC and WAXS measurements were performed by Qiao *et. al.*, reporting that Form II to I transition of PB-1 can be regarded as a nucleation-growth procedure.[23] By varying the molecular weight and lamellar thickness of PB-1, these authors demonstrated that the inter-crystalline links and tie chains play dual roles. On the one hand, the unbalanced stress between neighboring lamellae transmitted by the intercrystalline links accelerates the transition. On the other hand, the existence of intercrystalline links stabilizes the metastable Form II via hindering the translational movements of chains in the crystalline phase and slowing the relaxation of amorphous chains during phase transition.[24-26]

The Form II to I transition is also influenced remarkably by spatial confinement, such as in blends and thin films. Shieh et al.[8] observed that Form II to I transition is facilitated in PB-1-rich blends with polypropylene (*i*PP) possibly because the helical conformation of the α phase of *i*PP is similar to that of Form I of PB-1. Later, Wang et al.[27] found that Form I' could nucleate at the interface of PB-1/*i*PP immiscible blends when PB-1 droplets are finely dispersed in the *i*PP matrix. Reported results on PB-1 thin films regarding Form II to I transition are not always consistent.

This could be due to the coexistence of a surface layer and residual stresses together with a confinement effect. A decrease in Form II to I transition rate with decreasing film thickness has been reported,[28-30] however an increase in transition rate has also been observed.[31] A comparative study showed that the existence of evaporated carbon on PB-1 films retarded the transition to 120 days, which was attributed to a surface fixing effect occurring between the carbon and the polymer. On the other hand, the original film with the same thickness needs only 9 days to accomplish the transition under the same conditions, a time similar to that in bulk PB-1.[29]

Anodic aluminum oxide templates (AAO) with isolated, parallel, and uniform nanocylinders provide an ideal environment to study polymer crystallization under nanoconfinement.[32-36] Within AAO templates, the nucleation mechanism changes from heterogeneous to homogeneous or surface nucleation.[37-39] An anisotropic crystalline morphology is generally observed which is related to thermodynamic stability,[40] crystal growth kinetics,[41-43] and interfacial interactions.[44, 45] The crystallization kinetics of polymers within AAO exhibits a "nucleation-dominated kinetics".[46-48] Although the crystallization behavior from the melt state of polymers within AAO templates has been extensively studied, the influence of cylindrical confinement on the solid-solid crystalline transition is poorly understood.

In this work, PB-1 was chosen as a model polymer and the effects of nanoconfinement on the crystallization, melting, crystal orientation, with an emphasis on the solid-solid polymorphic transition of Form II to I, were studied. AAO templates covering the length scale of 30 nm to 400 nm in diameter were employed. The nucleation mechanism was evaluated by comparing the crystallization temperature (T_c) and glass transition temperature (T_g). The orientation of the crystals was characterized by grazing incident wide-angle X-ray scattering (GIWAXS). The Form II to I transition was monitored by time-dependent GIWAXS. The kinetics was evaluated by the classical Avrami equation. The results may provide new insights on the mechanism of the solid-solid transition in PB-1.

2. EXPERIMENTAL SECTION

2.1. Materials and Sample Preparation.

The PB-1 sample with a trade name of PB0800 was produced by LyondellBasell. The melt flow rate of the polymer is 200 g/10 min (190 ℃/2.16 kg). The sample has a weight-average (M_w) molecular weight of 77 kg/mol and a polydispersity of 3.0. The sample was used as received. AAO templates with pore diameters of 400 nm, 200 nm, 100 nm, 40 nm, and 30 nm and a pore length of approximately 100 μm were purchased from Shanghai Shangmu Technology Co. Ltd.

The polymer infiltration was carried out by using a home-made sample chamber with a temperature controller. The AAO templates were degassed under vacuum at 400 ℃ for 5 hours. After cooling down to room temperature, a piece of PB-1 film was placed on the surface of the AAO template and then annealed at 180 ℃, first under vacuum and then under a nitrogen atmosphere for 12 hours. The surface cleaning procedure was adapted from our previous publication: most of the residual polymer on the AAO surface was removed by a sharp blade at room temperature, and then the template was further cleaned with a soft cloth at 150 ℃. Multiple crystallization peaks would be observed in DSC if there is residual polymer on the template surface due to the percolation of pores that induces fractionated crystallization.[39]

2.2. Characterization.

A scanning electron microscope (SEM) (JSM-6700F JEOL) was used to observe the surface morphology of AAO and PB-1 nanorods (after dissolving the AAO templates). The microscope was operated at 5 kV. In order to observe PB-1, the infiltrated templates were immersed in an etching solution composed of chromium trioxide (CrO_3, 4.5 g), phosphoric acid (H_3PO_4, 3.5 mL), and water (96.5 mL), to dissolve the alumina.

A differential scanning calorimeter (DSC Q 200, TA) was employed to investigate thermal transitions during crystallization and melting. The calorimeter was calibrated with indium. For each experiment, we used around 5 mg of infiltrated samples including the aluminum base. The scanning range was between -60 and 180 ℃ and the heating/cooling rate was 10 ℃/min. The samples were protected by high purity nitrogen to avoid degradation.

A small and wide-angle X-ray scattering system (Xeuss 2.0, Xenocs SA) was used for the GIWAXS measurement. A Cu Kα X-ray source (GeniX3D) (50 kV, 0.6 mA) was used. The

wavelength of the radiation was 1.5418 Å. The detector we used was Pilatus 300 K (DECTRIS, Swiss). The detector contained 487 × 619 pixels with a size of 172 × 172 μm^2. The incident angle was set to 2°. The exposure times were 5 min and 30 min for bulk and infiltrated PB-1, respectively.

3. RESULTS AND DISCUSSION

3.1. Morphology of PB-1 Nanorods.

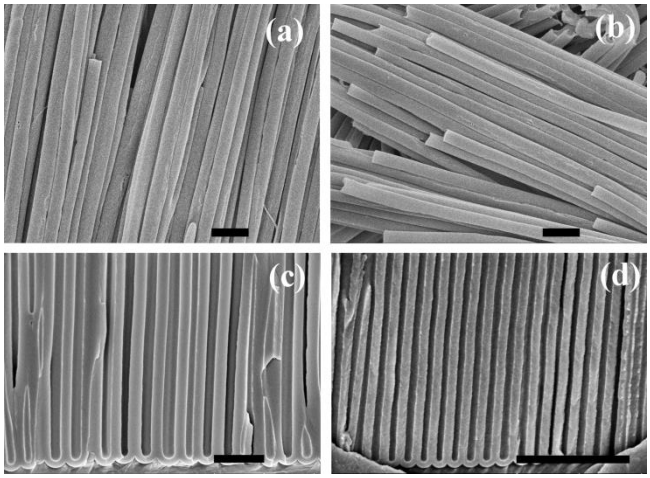

Figure 1. SEM images of PB-1 rods released from 400 nm AAO (a) and (b) and cross-sectional images of AAO with pore diameters of 200 nm (c) and 100 nm (d). The scale bars correspond to 1 μm.

Figure 1a and b display the morphology of the PB-1 nanorods extracted from the 400 nm AAO template (by dissolving the alumina). It is seen that the PB-1 rods are homogeneous and straight. Figure 1c and d show a side view of the templates. The results indicate that AAO template provides an ideal confining environment to get uniform parallel isolated nanocylinders.

3.2. Melting and Crystallization Behaviors.

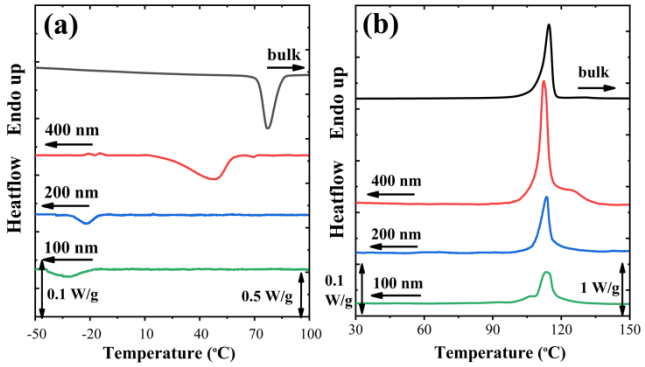

Figure 2. Cooling (a) and subsequent heating (b) DSC curves (both at 10 ℃/min) of bulk and infiltrated PB-1 within AAO templates.

Table 1. Crystallization and melting temperatures of bulk and infiltrated PB-1.

sample	T_m (℃)	T_c (℃)
bulk	114.6/130.5	75
400 nm	112.2/125.4	48
200 nm	113.5	-22.4
100 nm	113.8	-32.3

Figure 2 shows the DSC curves of bulk and infiltrated PB-1 within AAO pores. The crystallization (T_c) and subsequent melting temperatures (T_m) are summarized in Table 1. All the samples show similar melting T_m but very different T_c. According to the literature, the T_g of PB-1 is ~ -30 ℃ (by DSC).[10, 49] The T_c values of the infiltrated PB-1 samples within 200 nm and 100 nm templates are very close to T_g, i.e, at the maximum possible supercoolings available to the material.[38] Therefore, it is highly probable that the samples within AAO with diameters smaller than 200 nm crystallize *via* homogeneous nucleation. Similar behavior has been reported for infiltrated PEO[40] and PCL[39].

The samples within smaller AAO pores do not show clear crystallization peaks in their corresponding DSC scans because of the small amount of material infiltrated. It is noted that the 400 nm sample exhibits two endothermic peaks (Figure. 2b). The higher temperature peak corresponds to a small fraction of Form I that are either produced during cooling or transformed from From II during the test (0.5 ~ 1 h).

3.3. Crystal Structure and Orientation of PB-1 in Nanodomains.

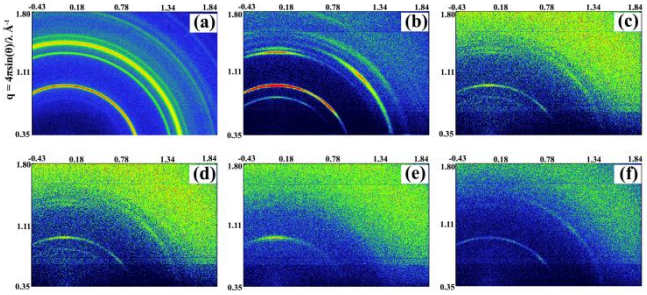

Figure 3. GIWAXS patterns of bulk (a) and infiltrated PB-1 within 400 nm (b), 200 nm (c), 100 nm (d), 40 nm (e), 30 nm (f) AAO templates after cooling from melt to -60 ℃ at 10 ℃/min.

To investigate the orientation of the confined PB-1 samples, 2D GIWAXS experiments were performed. The samples were first heated to 180 ℃ to erase the thermal history and then cooled to -60 ℃. Figure 3 shows that bulk PB-1 exhibits an isotropic pattern with predominant Form II crystal reflections. On the other hand, arcs are seen for infiltrated samples in Figure 3 indicating the existence of preferred orientation.

The 1D intensity curves are shown in Figure 4. According to the crystallographic structure of PB-1 in the literature,[7] the peaks at q = 0.85 Å^{-1}, 1.21 Å^{-1}, and 1.31 Å^{-1}, can be assigned to the (200), (220) and (213) reflections of Form II. The peak at q = 0.71 Å^{-1} for the 400 nm sample corresponds to the (110) reflection of Form I. Except for the 400 nm sample, all the other samples are mainly composed of Form II crystals.

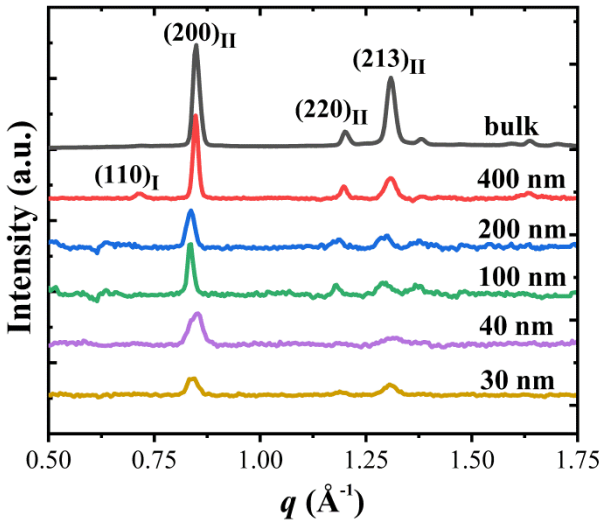

Figure 4. 1D intensity profiles of bulk and infiltrated PB-1 within AAO templates.

The orientation of polymer crystals within 1D nanocylinders has been a subject of intense investigation.[41-43, 50, 51] It is noticed in Figure 3 that the $(200)_{II}$, $(220)_{II}$ and $(213)_{II}$ reflections of the infiltrated samples have several maxima at different azimuthal angles. As an example, the azimuthal plots of the reflections of the 400 nm sample before and after annealing are displayed in Figure 5. For the melt crystallized sample, maxima are located at the meridian (ϕ = 0 °) for the $(200)_{II}$ and $(220)_{II}$ reflections. Another maximum at ϕ = 45 ° is seen for the $(200)_{II}$ reflection. For the $(213)_{II}$ reflection, a single maximum is observed at ϕ = 45 °. The infiltrated samples within smaller pores show similar features. As shown in Figure 5(c, d), after annealed for 100 days, the $(110)_{I}$ and $(220)_{I}$ reflections both have two peaks at ϕ = 0 ° and 29 °. The $(211)_{I}$ reflection has a maximum at ϕ = 45 °. The angle of a plane to the normal of AAO (φ) can be estimated using the Polanyi equation[52]:

$$\cos\varphi = \cos\theta\cos\phi$$

where θ is the half Bragg angle and ϕ is the azimuthal angle. The results are shown in Table 2. Because the θ values are below 10 °, the φ values are very close to ϕ values.

Table 2. The Parameters for Calculating the Angles between the Plane Normal to the Pore Axis for PB-1.

plane	θ (°)	ϕ (°)	φ (°)
$(200)_{II}$	5.99	45	45.3
$(213)_{II}$	9.25	45	45.7
$(110)_{I}$	5.00	29	29.4
$(211)_{I}$	10.3	45	45.9

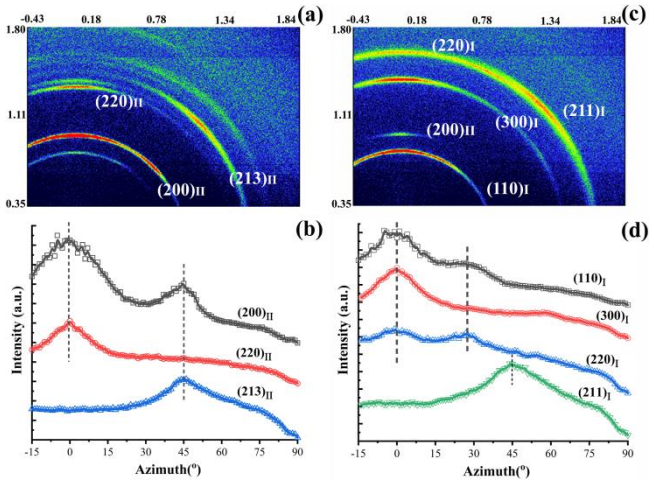

Figure 5. GIWAXS patterns (a, c) and azimuthal intensity profiles (b, d) of infiltrated PB-1 within 400 nm AAO templates after cooling from the melt (a, b) and after annealed at room temperature for 100 days (c, d). The meridian is defined as ϕ = 0 º.

Table 3 lists the angles between the different planes of Form II/I crystals according to the lattice parameters reported.[7] The angles of $(200)_{II}$ and $(213)_{II}$ to $(220)_{II}$ are 45 ° and 46.2 ° respectively, which agree with the φ values in Table 2. The azimuthal intensity distributions agree well with the combination of two uniaxial orientations for the Form II, i.e., the $(200)_{II}/(220)_{II}$ perpendicular to (⊥) the pore axis. As for Form I, the $(110)_I/(220)_I$ peak at ϕ = 29 º, and the $(211)_I$ at 45 ° correspond to a preferred orientation structure with the $(300)_I$ ⊥ pore axis. The crystallographic relationship of different planes indicates the orientation mode is a mixture of the $(300)_I/(110)_I$ ⊥ pore axis. Since we are only interested in the directions, both of the orientation of Form II and I can be assigned to the (100)/(110) ⊥ pore axis or the reciprocal <100>*/<110>* direction parallel to (∥) the pore axis. Mixed orientations have been observed frequently in crystalline polymers confined within AAO pores. It has been realized that the relative growth rate of different crystal planes determines the overall orientation in the region where multiple nuclei coexist within one nanocylinder.[42, 43]

It is known that the Form II to I transition exhibits a crystallographic matching relationship between the two crystalline modifications with a common (110) plane.[7, 53-56] The orientation of PB-1 within AAO templates exhibits a similar relationship. For example, the $(110)_I$ and $(220)_{II}$ align parallel to each other.

Table 3. The *d*-spacings and Interplanner Angles for PB-1.

plane	200_{II}	220_{II}	213_{II}	110_{I}	300_{I}	211_{I}
d calc (Å)	7.45	5.27	4.86	8.77	5.06	4.30
d obsd (Å)	7.39	5.19	4.80	8.85	5.07	4.30
angle to 200_{II}	-	45	49.3			
angle to 220_{II}	45	-	46.2			
angle to 213_{II}	49.3	46.2	-			
angle to 110_{I}				-	30	42.7
angle to 300_{I}				30	-	45
angle to 211_{I}				42.7	45	-

3.4. Crystal Transition Kinetics during Annealing.

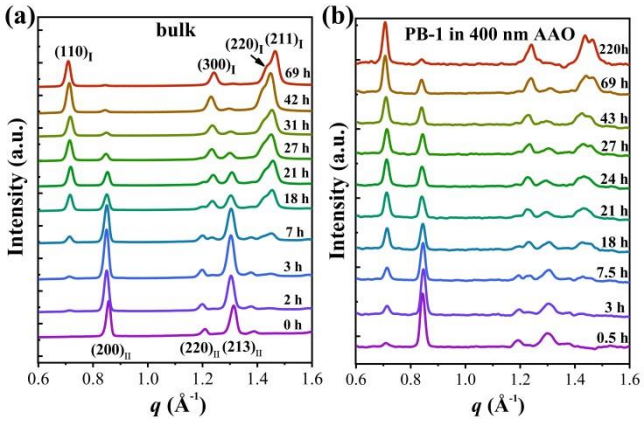

Figure 6. 1D intensity profiles of the bulk and infiltrated PB-1 within 400 nm AAO during annealing at room temperature.

It is interesting to observe how confinement influences the crystal-crystal polymorphic transition in PB-1. Figure 6 shows the GIWAXS of bulk and infiltrated PB-1 within AAO templates during annealing at room temperature. For bulk PB-1, the initial sample only shows the reflections of Form II, including the $(200)_{II}$, $(220)_{II}$ and $(213)_{II}$. During annealing, typical diffraction peaks of Form I appear, $(110)_{I}$, $(300)_{I}$ and $(220)_{I}$, located at q = 0.71 Å, 1.24 Å, and 1.46 Å, respectively. The intensities of the $(200)_{II}$, $(220)_{II}$, $(213)_{II}$ peaks decrease with annealing time gradually, while the intensities of the peaks corresponding to Form I increase. When the annealing time reaches 69 h, the Form II to I transition is almost complete for bulk PB-1, which agrees well with the previous studies.[57] Although the initial 400 nm sample contains a certain

amount of Form I crystals, the Form II to I transition degree is lower than the bulk at long annealing time.

The content of Form I (X_I) can be estimated according to the formula:[23, 25]

$$X_I = \frac{I(110)_I}{I(110)_I + R * I(200)_{II}}$$

where $I(110)_I$ and $I(200)_{II}$ are the integrated areas of the $(110)_I$ and $(200)_{II}$ diffraction peaks; R is a correction parameter that considers both the structure factors and Lorentz-polarization factors, and it is set to 0.67 according to Men et al.[25]

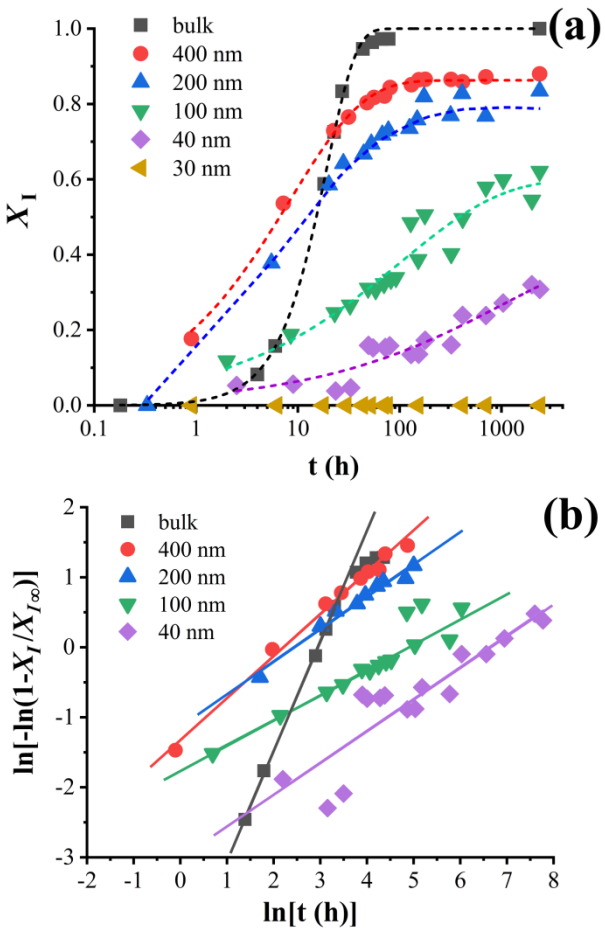

Figure 7. The evolution of X_I as a function of annealing time at room temperature (a) and the Avrami plot (b) of the bulk and infiltrated PB-1 within AAO templates.

Figure 7a shows the evolution of the content of Form I crystals (X_I) during annealing at room temperature. The longest annealing time is 2000 hours (~ 3 months). The general observation is

that the transition slows down with decreasing AAO pore diameter. The data points for the solid-solid transformation can be fitted with the Avrami equation:[58, 59]

$$\frac{X_I}{X_{I\infty}} = 1 - \exp[-k * (t - t_0)^n]$$

where *t* is the annealing time, t_0 is the induction time, *k* is the transformation rate constant and *n* is the Avrami index, $X_{I\infty}$ is a constant to describe the saturation of the transition degree. The Avrami index *n* can be expressed by the addition of two terms[60]:

$$n = n_n + n_{gd}$$

where n_n, ranging from 0 to 1 is related to the nucleation mechanism from instantaneous to sporadic and n_{gd} is related to the dimensionality of crystal growth (0 ~ 3). The equation can be rewritten in the form of Avrami plot:

$$\ln\left[-\ln\left(1 - \frac{X_I}{X_{I\infty}}\right)\right] = \ln(k) + n * \ln(t - t_0)$$

The half crystallization time can be obtained by:

$$\tau_{50\%} = \left(\frac{\ln 2}{k}\right)^{1/n}$$

The corresponding parameters are listed in Table 4. Bulk PB-1 shows an *n* of 1.52, comparable with a previous report.[23] This *n* value can be approximated to 2 and explained as a result of sporadic nucleation ($n_n = 1$) of 1D structures ($n_{gd} = 1$). Rod-like growth of Form I has been confirmed by Chau et al.[28] Different from the melt crystallization which is normally triggered by the heterogeneities, the nucleation of Form I within Form II crystalline matrix has been assigned to homogeneous nucleation.[23]

In the case where crystallization from the melt occurs within AAO nanopores via a homogeneous nucleation mechanism ($n_n = 1$), the overall kinetics is dominated by nucleation, as growth is much faster (n_{gd} = 0). Hence, *n* = 1 is expected. In the present case, it is the kinetics of the solid-solid transformation which is being modeled with the Avrami equation, not the overall crystallization from the melt. Nevertheless, the *n* values are lower than 1 in all cases (Table 4) and

they decrease with pore size reduction. If it is considered that the nucleation is the dominant step ($n_{gd} = 0$), then the low *n* values can be interpreted as due to a nucleation mechanism between sporadic and instantaneous[46] or due to sporadic nucleation and growth of multiple crystal planes with drastically different growth rates within one pore.[48]

The plateau transition degree $X_{I\infty}$ is plotted in Figure 8b and it can be observed that it decreases monotonically with decreasing diameter of AAO nanopores. The transition rate exhibits an interesting dependence on the confining environment size. Specifically, the $\tau_{50\%}$ for the bulk sample is 15.3 h. For infiltrated PB-1 within 400 nm AAO, the $\tau_{50\%}$ is 4.5 h, much shorter than that of the bulk. When decreasing the pore diameter, the $\tau_{50\%}$ increases. The infiltrated PB-1 within 400 nm AAO has the minimum $\tau_{50\%}$ and highest *k* value, as shown in Table 4 and Figure 8a.

Table 4. Fitting Results of the Crystal Transition during Room Temperature Annealing.

sample	$X_{I\infty}$	*k* (h^{-n})	*n*	$\tau_{50\%}$ (h)
bulk	1	0.011 ± 0.002	1.52 ± 0.07	15.3 ± 2.6
400 nm	0.863 ± 0.004	0.28 ± 0.02	0.60 + 0.02	4.5 ± 0.6
200 nm	0.79 ± 0.02	0.20 ± 0.04	0.61 ± 0.07	7.7 ± 3.1
100 nm	0.60 ± 0.04	0.13 ± 0.03	0.44 ± 0.07	45 ± 36
40 nm	0.4 ± 0.2	0.07 ± 0.02	0.39 ± 0.11	357 ± 648

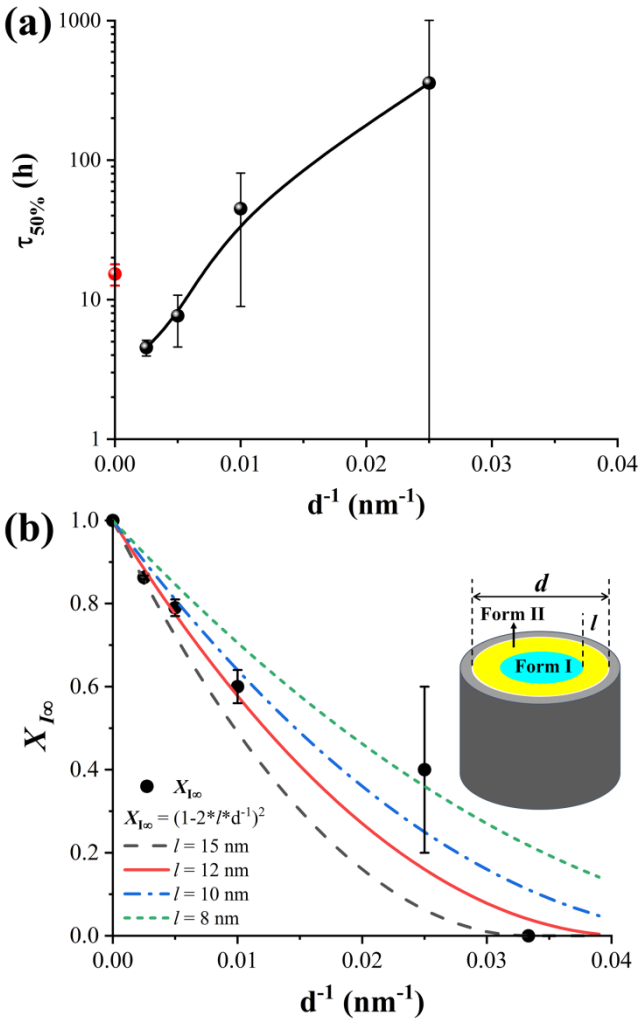

Figure 8. The change of $\tau_{50\%}$ (a) and $X_{I\infty}$ (b) as a function of AAO pore diameters. The curves in (b) represent the values calculated by $X_{I\infty} = (1 - 2 * l * d^{-1})^2$ where l is the thickness of a hypothetical interfacial layer that cannot transform into Form I and d is the diameter of the AAO pores.

3.6. Mechanism of the Crystal Transition under Confinement.

For polymer crystallization from the melt under confinement, two factors should be taken into account. The first is the change in nucleation mechanism, from heterogeneous to surface or homogeneous nucleation. Second, the crystal growth is spatially restricted within the nanodomains (hence the time needed for crystal growth to fill a pore is much shorter than the time to form a nucleus) and the overall crystallization kinetics is dominated by nucleation.[32, 46] The above two factors generally lead to a much lower overall crystallization rate from the melt as compared to the

bulk under the same conditions.[46, 48] Our results on the Form II to I transition of PB-1 under confinement within AAO are different, as we are dealing with a solid-solid transformation that can be affected by stress.

External or internal stresses play a significant role in the nucleation of Form I within a Form II matrix.[3, 5, 18, 21] Solution-grown crystals have a minimum mechanical disturbance. Therefore, the transition rate is so small that the mono-lamellar crystals do not transform after one month[61] or even stay in Form II for more than 1 year.[30] For molded rods, Choi. et al.[62] reported that Form II to I transition is faster in the core region than in the outer layer, which is explained by the larger residual quench stress in the core.

As for our system, the linear thermal expansion coefficients were estimated to be 2.2 ~ 2.6 × 10^{-4} and 1.2 ~ 1.4 × 10^{-4} $℃^{-1}$ for amorphous[16] and crystalline[63] PB-1, respectively, which are 2 orders of magnitude larger than those of alumina (5.4 ~ 6.4 × 10^{-6} $℃^{-1}$, 25 ~200 ℃[64]). The infiltrated PB-1 within AAO is expected to endure significant stresses due to the mismatch in the thermal expansion coefficients. Specifically, such stress is expected to be generated after solidification of PB-1, therefore a lower crystallization temperature may produce less internal stress. Since the 400 nm sample has the highest T_c among the infiltrated samples, the stress experienced by the PB-1 rods enhanced the nucleation of the 400 nm sample as compared to the bulk sample. With the decreasing diameter of AAO pores, the transition rate decreases, possibly due to two factors. First, for homogeneous nucleation, smaller volumes have lower nucleation probability. Secondly, the possible lower stress in the smaller pores can be another reason for the lower transition rate for PB-1 in smaller pores. We would like to point out that internal stress is closely related to the intercrystalline links and tie chains, which is strongly influenced by the lamellar thickness. For the bulk PB-1, the lamellar thickness of Form II can be fixed by setting the same isothermal crystallization temperature, as shown by Qiao *et al.*[24, 25] However, in the current situation, because the confinement effect, it is not possible to crystallize the sample at the same temperature. Therefore, we could not separate the effect of internal stress from the confinement effect.

The degree of transition for infinite time ($X_{I\infty}$) decreases dramatically with decreasing diameter.

It is known that the degree of transition for bulk PB-1 reaches a plateau value[25] that depends on the crystallization condition and molecular weight. Cavallo et al. observed there were residual Form II crystals remained after mechanical deformation.[18] However, the plateau values of transition for bulk PB-1 are much higher than the values we observed. The continuous decrease of $X_{I\infty}$ could indicate the existence of an interfacial layer in the vicinity of the AAO wall that cannot transform to Form I.

A test to corroborate the hypothesis outlined above can consist of a plot of the volume fraction of the "core PB-1" as a function of pore diameter (d):

$$X_{I\infty} = (1 - 2 * l * d^{-1})^2$$

In this equation, it is assumed that only the core part of PB-1 nanocylinder can transform to Form I, and that the untransformed fraction is related to a stable interfacial Form II layer at the AAO cylinder surface of constant thickness, l. Therefore, the trend of $X_{I\infty}$ has been calculated as a function of pore diameter, assuming different thicknesses of the interfacial layer. As shown in Figure 8b, the red line (l = 12 nm) fits the data points of bulk, 400 nm, 200 nm, and 100 nm satisfactorily. The mobility of chain segments close to an interface can be hindered due to adsorption during annealing,[65-67] which can significantly slow down or even eliminate the transition. When the diameter of AAO decreased to 40 nm or 30 nm, the core diameter would be 16 nm and 6 nm assuming l = 12 nm, respectively. According to the literature,[24, 25, 68] the lamellar thickness of PB-1 is in the range of 12 ~ 25 nm depending on the molecular weight and crystallization condition. Therefore, when the diameter is approaching the lamellar thickness, other effects should be considered. For example, only one lamella may be formed within the 30 nm pores, therefore it is expected it should not have "intercrystalline links"[24] to transmit the stress, which is similar to the case of solution-grown crystals.[30, 61] The origin of the stable Form II fractions and the possible existence of interlayer have to be further investigated.

4. CONCLUSIONS

Crystallization of PB-1 within nanoporous AAO templates exhibited several common features of confined crystallization. Upon cooling from the melt of the infiltrated PB-1, within AAO

templates with diameters lower than 200 nm, Form II was formed directly via homogeneous nucleation. The Form II and I crystals showed a common mixed-orientation: the reciprocal <100>*/<110>* ∥ pore axis. The polymorphic Form II to I transition during annealing was investigated by GIWAXS. The transition rate of infiltrated PB-1 within 400 nm AAO was unexpectedly higher than that of the bulk. This result was explained by the stress generated inside the nanopores between PB-1 and AAO due to the mismatch in thermal expansion coefficients. Slower Form II to I transition was observed when the diameter of AAO decreased. The transition degree decreased with decreasing pore diameter and was completely inhibited for PB-1 infiltrated within 30 nm AAO. A stable Form II interfacial layer was postulated to account for the observation.

ACKNOWLEDGEMENTS

This work is supported by the National Key R&D Program of China (2017YFE0117800) and the National Natural Science Foundation of China (21873109 and 21922308). We acknowledge sponsorship from the European Union's Horizon 2020 research and innovation program under the Marie Sklodowska-Curie grant agreement No 778092. G. L. is grateful to the Youth Innovation Promotion Association of the Chinese Academy of Sciences (Y201908).

REFERENCES

1. Luciani, L.; Seppälä, J.; Löfgren, B. Poly-1-butene: Its preparation, properties and challenges. *Prog. Polym. Sci.* **1988,** 13 (1), 37-62 DOI: 10.1016/0079-6700(88)90010-X.
2. Xin, R.; Zhang, J.; Sun, X.; Li, H.; Ren, Z.; Yan, S. Polymorphic Behavior and Phase Transition of Poly(1-Butene) and Its Copolymers. *Polymers* **2018,** 10 (5), DOI: 10.3390/polym10050556.
3. Xu, Y.; Liu, T.; Li, L.; Li, D.-c.; Yuan, W.-k.; Zhao, L. Controlling crystal phase transition from form II to I in isotactic poly-1-butene using CO2. *Polymer* **2012,** 53 (26), 6102-6111 DOI: 10.1016/j.polymer.2012.10.049.
4. Su, F.; Li, X.; Zhou, W.; Zhu, S.; Ji, Y.; Wang, Z.; Qi, Z.; Li, L. Direct Formation of Isotactic Poly(1-butene) Form I Crystal from Memorized Ordered Melt. *Macromolecules* **2013,** 46 (18), 7399-7405 DOI: 10.1021/ma400952r.
5. Liu, Y.; Cui, K.; Tian, N.; Zhou, W.; Meng, L.; Li, L.; Ma, Z.; Wang, X. Stretch-Induced Crystal–Crystal Transition of Polybutene-1: An in Situ Synchrotron Radiation Wide-Angle X-ray Scattering Study. *Macromolecules* **2012,** 45 (6), 2764-2772 DOI: 10.1021/ma2026513.
6. Maruyama, M.; Sakamoto, Y.; Nozaki, K.; Yamamoto, T.; Kajioka, H.; Toda, A.; Yamada, K. Kinetic study of the II–I phase transition of isotactic polybutene-1. *Polymer* **2010,** 51 (23), 5532-5538 DOI: 10.1016/j.polymer.2010.09.066.

7. Tashiro, K.; Hu, J.; Wang, H.; Hanesaka, M.; Saiani, A. Refinement of the Crystal Structures of Forms I and II of Isotactic Polybutene-1 and a Proposal of Phase Transition Mechanism between Them. *Macromolecules* **2016,** 49 (4), 1392-1404 DOI: 10.1021/acs.macromol.5b02785.

8. Shieh, Y. T.; Lee, M. S.; Chen, S. A. Crystallization behavior, crystal transformation, and morphology of polypropylene/polybutene-1 blends. *Polymer* **2001,** 42 (9), 4439-4448 DOI: 10.1016/S0032-3861(00)00567-X.

9. De Rosa, C.; Auriemma, F.; Villani, M.; Ruiz de Ballesteros, O.; Di Girolamo, R.; Tarallo, O.; Malafronte, A. Mechanical Properties and Stress-Induced Phase Transformations of Metallocene Isotactic Poly(1-butene): The Influence of Stereodefects. *Macromolecules* **2014,** 47 (3), 1053-1064 DOI: 10.1021/ma402239k.

10. Li, J.; Wang, D.; Cai, X.; Zhou, C.; de Claville Christiansen, J.; Sørensen, T.; Yu, D.; Xue, M.; Jiang, S. Conformation Selected Direct Formation of Form I in Isotactic Poly(butene-1). *Cryst. Growth Des.* **2018,** 18 (4), 2525-2537 DOI: 10.1021/acs.cgd.8b00119.

11. Zhang, B.; Yang, D.; Yan, S. Direct formation of form I poly(1-butene) single crystals from melt crystallization in ultrathin films. *J. Polym. Sci., Part B: Polym. Phys.* **2002,** 40 (23), 2641-2645 DOI: 10.1002/polb.10327.

12. Yamashita, M.; Hoshino, A.; Kato, M. Isotactic poly(butene-1) trigonal crystal growth in the melt. *J. Polym. Sci., Part B: Polym. Phys.* **2007,** 45 (6), 684-697 DOI: 10.1002/polb.21052.

13. Wang, Y.; Lu, Y.; Zhao, J.; Jiang, Z.; Men, Y. Direct Formation of Different Crystalline Forms in Butene-1/Ethylene Copolymer via Manipulating Melt Temperature. *Macromolecules* **2014,** 47 (24), 8653-8662 DOI: 10.1021/ma5019796.

14. Wang, Y.-T.; Liu, P.-T.; Lu, Y.; Men, Y.-F. Mechanism of polymorph selection during crystallization of random butene-1/ethylene copolymer. *Chin. J. Polym. Sci.* **2016,** 34 (8), 1014-1020 DOI: 10.1007/s10118-016-1802-8.

15. Lai, Y.; Men, Y. Polymorph selection during crystallization of random copolymers. *Eur. Polym. J.* **2018,** 101, 218-224 DOI: 10.1016/j.eurpolymj.2018.02.038.

16. Boor Jr., J.; Mitchell, J. C. Kinetics of crystallization and a crystal-crystal transition in poly-1-butene. *J. Polym. Sci., Part A: Gen. Pap.* **1963,** 1 (1), 59-84 DOI: 10.1002/pol.1963.100010106.

17. Nakafuku, C.; Miyaki, T. Effect of pressure on the melting and crystallization behaviour of isotactic polybutene-1. *Polymer* **1983,** 24 (2), 141-148 DOI: 10.1016/0032-3861(83)90124-6.

18. Cavallo, D.; Kanters, M. J. W.; Caelers, H. J. M.; Portale, G.; Govaert, L. E. Kinetics of the Polymorphic Transition in Isotactic Poly(1-butene) under Uniaxial Extension. New Insights From Designed Mechanical histories. *Macromolecules* **2014,** 47 (9), 3033-3040 DOI: 10.1021/ma500281f.

19. Nakamura, K.; Aoike, T.; Usaka, K.; Kanamoto, T. Phase Transformation in Poly(1-butene) upon Drawing. *Macromolecules* **1999,** 32 (15), 4975-4982 DOI: 10.1021/ma981735f.

20. Tanaka, A.; Sugimoto, N.; Asada, T.; Onogi, S. Orientation and Crystal Transformation in Polybutene-1 under Stress Relaxation. *Poly. J.* **1975,** 7 (5), 529-537 DOI: 10.1295/polymj.7.529.

21. Chen, W.; Li, X.; Li, H.; Su, F.; Zhou, W.; Li, L. Deformation-induced crystal–crystal transition of polybutene-1: an in situ FTIR imaging study. *J. Mater. Sci.* **2013,** 48 (14), 4925-4933 DOI: 10.1007/s10853-013-7273-1.

22. Azzurri, F.; Alfonso, G. C.; Gómez, M. A.; Martì, M. C.; Ellis, G.; Marco, C. Polymorphic Transformation in Isotactic 1-Butene/Ethylene Copolymers. *Macromolecules* **2004,** 37 (10), 3755-3762 DOI: 10.1021/ma0358327.

23. Qiao, Y.; Wang, Q.; Men, Y. Kinetics of Nucleation and Growth of Form II to I Polymorphic

Transition in Polybutene-1 as Revealed by Stepwise Annealing. *Macromolecules* **2016,** 49 (14), 5126-5136 DOI: 10.1021/acs.macromol.6b00862.

24. Qiao, Y.; Men, Y. Intercrystalline Links Determined Kinetics of Form II to I Polymorphic Transition in Polybutene-1. *Macromolecules* **2017,** 50 (14), 5490-5497 DOI: 10.1021/acs.macromol.7b00771.

25. Qiao, Y.; Wang, H.; Men, Y. Retardance of Form II to Form I Transition in Polybutene-1 at Late Stage: A Proposal of a New Mechanism. *Macromolecules* **2018,** 51 (6), 2232-2239 DOI: 10.1021/acs.macromol.7b02481.

26. Qiao, Y.; Yang, F.; Lu, Y.; Liu, P.; Li, Y.; Men, Y. Spontaneous Form II to I Transition in Low Molar Mass Polybutene-1 at Crystallization Temperature Reveals Stabilization Role of Intercrystalline Links and Entanglements for Metastable Form II Crystals. *Macromolecules* **2018,** 51 (20), 8298-8305 DOI: 10.1021/acs.macromol.8b01795.

27. Wang, Z.; Dong, X.; Liu, G.; Xing, Q.; Cavallo, D.; Jiang, Q.; Müller, A. J.; Wang, D. Interfacial nucleation in iPP/PB-1 blends promotes the formation of polybutene-1 trigonal crystals. *Polymer* **2018,** 138, 396-406 DOI: 10.1016/j.polymer.2018.01.078.

28. Chau, K. W.; Yang, Y. C.; Geil, P. H. Tetragonal → twinned hexagonal crystal phase transformation in polybutene-1. *J. Mater. Sci.* **1986,** 21 (9), 3002-3014 DOI: 10.1007/BF00553329.

29. Lü, K.; Yang, D. Stabilization of metastable phase II of isotactic polybutene-1 by coated carbon. *Polym. Bull.* **2006,** 58 (4), 731-736 DOI: 10.1007/s00289-006-0705-1.

30. Gohil, R. M.; Miles, M. J.; Petermann, J. On the molecular mechanism of the crystal transformation (tetragonal-hexagonal) in polybutene-1. *J. Macromol. Sci. B* **2006,** 21 (2), 189-201 DOI: 10.1080/00222348208204934.

31. Clampitt, B. H.; Hughes, R. H. Differential thermal analysis of polybutene-1. *J. Polym. Sci., Part C: Polym. Symp.* **1964,** 6 (1), 43-51 DOI: 10.1002/polc.5070060107.

32. Michell, R. M.; Blaszczyk-Lezak, I.; Mijangos, C.; Muller, A. J. Confined Crystallization of Polymers within Anodic Aluminum Oxide Templates. *J. Polym. Sci., Part B: Polym. Phys.* **2014,** 52 (18), 1179-1194 DOI: 10.1002/polb.23553.

33. Michell, R. M.; Müller, A. J. Confined crystallization of polymeric materials. *Prog. Polym. Sci.* **2016,** 54, 183-213 DOI: 10.1016/j.progpolymsci.2015.10.007.

34. Samanta, P.; Liu, C.-L.; Nandan, B.; Chen, H.-L., Chapter 13 - Crystallization of Polymers in Confined Space A2 - Thomas, Sabu. In *Crystallization in Multiphase Polymer Systems*, P, M. A., Gowd, E. B., Kalarikkal, N., Eds. Elsevier: 2018; pp 367-431.

35. Wu, H.; Higaki, Y.; Takahara, A. Molecular self-assembly of one-dimensional polymer nanostructures in nanopores of anodic alumina oxide templates. *Prog. Polym. Sci.* **2018,** 77, 95-117 DOI: 10.1016/j.progpolymsci.2017.10.004.

36. Liu, G.; Shi, G.; Wang, D. Research Progress on Polymer Crystallization Confined within Nano-porous AAO Templates. *Acta Polym. Sin.* **2020,** 51 (5), 501-516 DOI: 10.11777/j.issn1000-3304.2020.20003.

37. Duran, H.; Steinhart, M.; Butt, H.-J.; Floudas, G. From Heterogeneous to Homogeneous Nucleation of Isotactic Poly(propylene) Confined to Nanoporous Alumina. *Nano Lett.* **2011,** 11 (4), 1671-1675 DOI: 10.1021/nl200153c.

38. Michell, R. M.; Lorenzo, A. T.; Müller, A. J.; Lin, M.-C.; Chen, H.-L.; Blaszczyk-Lezak, I.; Martín, J.; Mijangos, C. The Crystallization of Confined Polymers and Block Copolymers Infiltrated Within Alumina Nanotube Templates. *Macromolecules* **2012,** (45), 1517-1528 DOI:

10.1021/ma202327f.

39. Shi, G.; Liu, G.; Su, C.; Chen, H.; Chen, Y.; Su, Y.; Müller, A. J.; Wang, D. Reexamining the Crystallization of Poly(ε-caprolactone) and Isotactic Polypropylene under Hard Confinement: Nucleation and Orientation. *Macromolecules* **2017,** 50 (22), 9015-9023 DOI: 10.1021/acs.macromol.7b02284.

40. Guan, Y.; Liu, G.; Gao, P.; Li, L.; Ding, G.; Wang, D. Manipulating Crystal Orientation of Poly(ethylene oxide) by Nanopores. *ACS Macro Lett.* **2013,** 2 (3), 181-184 DOI: 10.1021/mz300592v.

41. Steinhart, M.; Goring, P.; Dernaika, H.; Prabhukaran, M.; Gosele, U.; Hempel, E.; Thurn-Albrecht, T. Coherent kinetic control over crystal orientation in macroscopic ensembles of polymer nanorods and nanotubes. *Phys. Rev. Lett.* **2006,** 97 (2), 027801 DOI: 10.1103/PhysRevLett.97.027801.

42. Su, C.; Shi, G.; Li, X.; Zhang, X.; Müller, A. J.; Wang, D.; Liu, G. Uniaxial and Mixed Orientations of Poly(ethylene oxide) in Nanoporous Alumina Studied by X-ray Pole Figure Analysis. *Macromolecules* **2018,** 51 (23), 9484-9493 DOI: 10.1021/acs.macromol.8b01801.

43. Su, C.; Shi, G.; Wang, D.; Liu, G. A Model for the Crystal Orientation of Polymers Confined in 1D Nanocylinders. *Acta Polym. Sin.* **2019,** 50 (3), 281-290 DOI: 10.11777/j.issn1000-3304.2018.18218.

44. Ma, Y.; Hu, W.; Hobbs, J.; Reiter, G. Understanding crystal orientation in quasi-one-dimensional polymer systems. *Soft Matter* **2008,** 4 (3), 540-543 DOI: 10.1039/B715065B.

45. Wu, H.; Wang, W.; Huang, Y.; Su, Z. Orientation of Syndiotactic Polystyrene Crystallized in Cylindrical Nanopores. *Macromol. Rapid Commun.* **2009,** 30, 194-198 DOI: 10.1002/marc.200800626.

46. Michell, R. M.; Blaszczyk-Lezak, I.; Mijangos, C.; Müller, A. J. Confinement Effects on Polymer Crystallization: from Droplets to Alumina Nanopores. *Polymer* **2013,** 54 (16), 4059-4077 DOI: 10.1016/j.polymer.2013.05.029.

47. Shin, K.; Woo, E.; Jeong, Y. G.; Kim, C.; Huh, J.; Kim, K.-W. Crystalline Structures, Melting, and Crystallization of Linear Polyethylene in Cylindrical Nanopores. *Macromolecules* **2007,** 40, 6617-6623 DOI: 10.1021/ma070994e.

48. Su, C.; Chen, Y.; Shi, G.; Li, T.; Liu, G.; Müller, A. J.; Wang, D. Crystallization Kinetics of Poly(ethylene oxide) under Confinement in Nanoporous Alumina Studied by in Situ X-ray Scattering and Simulation. *Langmuir* **2019,** 35 (36), 11799-11808 DOI: 10.1021/acs.langmuir.9b01968.

49. An, C.; Lou, Y.; Li, Y.; Wang, B.; Pan, L.; Ma, Z.; Li, Y. Unusual II–I Phase Transition Behavior of Polybutene-1 Ionomers in the Presence of Long-Chain Branch and Ionic Functional Groups. *Macromolecules* **2019,** 52 (12), 4634-4645 DOI: 10.1021/acs.macromol.9b00346.

50. Wu, H.; Wang, W.; Yang, H.; Su, Z. Crystallization and Orientation of Syndiotactic Polystyrene in Nanorods. *Macromolecules* **2007,** 40, 4244-4249 DOI: 10.1021/ma070564o.

51. Liu, C.-L.; Chen, H.-L. Variable Crystal Orientation of Poly(ethylene oxide) Confined within the Tubular Space Templated by Anodic Aluminum Oxide Nanochannels. *Macromolecules* **2017,** 50 (2), 631-641 DOI: 10.1021/acs.macromol.6b02347.

52. Polanyi, M. The X-ray fiber diagram. *Z Phys* **1921,** 7, 149-180 DOI: 10.1007/BF01332786.

53. Holland, V. F.; Miller, R. L. Isotactic Polybutene‐1 Single Crystals: Morphology. *J. Appl. Phys.* **1964,** 35 (11), 3241-3248 DOI: 10.1063/1.1713205.

54. Fujiwara, Y. II-I phase transformation of melt-crystallized oriented lamellae of polybutene-1 by shear deformation. *Polym. Bull.* **1985,** 13 (3), 253-258 DOI: 10.1007/BF00254659.

55. Kopp, S.; Wittmann, J. C.; Lotz, B. Epitaxial crystallization and crystalline polymorphism of poly(1-butene): form I. *Polymer* **1994,** 35 (5), 916-924 DOI: 10.1016/0032-3861(94)90933-4.

56. Tosaka, M.; Kamijo, T.; Tsuji, M.; Kohjiya, S.; Ogawa, T.; Isoda, S.; Kobayashi, T. High-Resolution Transmission Electron Microscopy of Crystal Transformation in Solution-Grown Lamellae of Isotactic Polybutene-1. *Macromolecules* **2000,** 33 (26), 9666-9672 DOI: 10.1021/ma001495f.

57. Wanjale, S. D.; Jog, J. P. Crystallization and phase transformation kinetics of poly(1-butene)/MWCNT nanocomposites. *Polymer* **2006,** 47 (18), 6414-6421 DOI: 10.1016/j.polymer.2006.07.011.

58. Avrami, M. Granulation, Phase Change, and Microstructure Kinetics of Phase Change. III. *J. Chem. Phys.* **1941,** 9 (2), 177-184 DOI: 10.1063/1.1750872.

59. Lorenzo, A. T.; Arnal, M. L.; Albuerne, J.; Müller, A. J. DSC isothermal polymer crystallization kinetics measurements and the use of the Avrami equation to fit the data: Guidelines to avoid common problems. *Polym. Test.* **2007,** 26 (2), 222-231 DOI: 10.1016/j.polymertesting.2006.10.005.

60. Balsamo, V.; Urdaneta, N.; Pérez, L.; Carrizales, P.; Abetz, V.; Müller, A. J. Effect of the polyethylene confinement and topology on its crystallisation within semicrystalline ABC triblock copolymers. *Eur. Polym. J.* **2004,** 40 (6), 1033-1049 DOI: 10.1016/j.eurpolymj.2004.01.009.

61. Kopp, S.; Wittmann, J. C.; Lotz, B. Phase II to phase I crystal transformation in polybutene-1 single crystals: a reinvestigation. *J. Mater. Sci.* **1994,** 29 (23), 6159-6166 DOI: 10.1007/BF00354556.

62. Choi, C.-H.; White, J. L. Crystal-crystal transformations in isotactic polybutene-1 oriented filaments and in thick molded rods. *Polym. Eng. Sci.* **2001,** 41 (6), 933-939 DOI: 10.1002/pen.10792.

63. Powers, J.; Hoffman, J. D.; Weeks, J. J.; Quinn, F. A., Jr. Crystallization Kinetics and Polymorphic Transformations in Polybutene-1. *J. Res. Natl. Bur. Stand. A Phys. Chem.* **1965,** 69A (4), 335-345 DOI: 10.6028/jres.069A.034.

64. COBLE, R. L.; KINGERY, W. D. Effect of Porosity on Physical Properties of Sintered Alumina. *J. Am. Ceram. Soc.* **1956,** 39 (11), 377-385 DOI: 10.1111/j.1151-2916.1956.tb15608.x.

65. Shi, G.; Guan, Y.; Liu, G.; Müller, A. J.; Wang, D. Segmental Dynamics Govern the Cold Crystallization of Poly(lactic acid) in Nanoporous Alumina. *Macromolecules* **2019,** 52 (18), 6904-6912 DOI: 10.1021/acs.macromol.9b00542.

66. Li, L.; Zhou, D.; Huang, D.; Xue, G. Double Glass Transition Temperatures of Poly(methyl methacrylate) Confined in Alumina Nanotube Templates. *Macromolecules* **2014,** 47 (1), 297-303 DOI: 10.1021/ma4020017.

67. Panagopoulou, A.; Napolitano, S. Irreversible Adsorption Governs the Equilibration of Thin Polymer Films. *Phys. Rev. Lett.* **2017,** 119 (9), 097801 DOI:10.1103/PhysRevLett.119.097801.

68. Wang, Y.; Jiang, Z.; Fu, L.; Lu, Y.; Men, Y. Stretching Temperature Dependency of Lamellar Thickness in Stress-Induced Localized Melting and Recrystallized Polybutene-1. *Macromolecules* **2013,** 46 (19), 7874-7879 DOI: 10.1021/ma401326g.

For Table of Contents of Use Only

Crystallization, Orientation and Solid-Solid Crystal Transition of Polybutene-1 Confined within Nanoporous Alumina

Guangyu Shi, Zefan Wang, Ming Wang, Guoming Liu*, Dario Cavallo, Alejandro J. Müller and Dujin Wang